MUST Journal of Research and Development (MJRD) Volume 7 Issue 2, June 2026
e ISSN 2683-6467 & p ISSN 2683-6475

Modelling and Optimisation of Resilience and Corrosion Rate of Aluminium 7075 Thin Plate during Surface Grinding

[1]Michael Kwabena Boadu*, [2]Anthony Agyei-Agyemang, [3]Prince Yaw Andoh and [4]Faisal Wahib Adam
[1]University for Development Studies, P.O Box TL 1882, Tamale, Ghana
[2,3,4]Kwame Nkrumah University of Science and Technology, PMB, Kumasi, Ghana
DOI: https://doi.org/10.62277/mjrd2026v7i20001

ARTICLE INFORMATION

Article History

Received: 27th July 2025
Revised: 05th January 2026
Accepted: 15th February 2026
Published: 15th March 2026

Keywords

Modeling
Optimization
Resilience
Corrosion Rate
Surface Grinding

ABSTRACT

The main goal of this work is to model and optimise the resilience and corrosion rate of Aluminium 7075 (AA7075) thin plate during surface grinding. AA7075 thin plates were ground with respect to the factorial design schedule, and their resilience and corrosion rate were determined from the DI-CP/V2 servo-hydraulic testing machine and the CS series electrochemical workstation, respectively. The Minitab statistical tool was utilised to analyse the data. Statistical analysis revealed that feed rate (absolute standardised effect = 8.68) and table speed (6.81) are the most influential factors affecting resilience, while the feed–grinding depth interaction (2.78) also contributes significantly. The interactions between table speed and feed, and between table speed and grinding depth, were not significant. For corrosion rate, feed and its interaction with grinding depth exhibited the strongest influence (10.94), followed by table speed (6.37) and the three-factor interaction (2.34), whereas other interactions were insignificant. The resilience model demonstrated good predictive capability (R^2 = 83.64%, adj. R^2 = 75.22%, pred. R^2 = 61.05%), while the corrosion rate model showed excellent predictive accuracy (R^2 = 99.20%, adj. R^2 = 98.42%, pred. R^2 = 96.78%). The optimal conditions were found to be low table speed (2.0 spm), low feed (1.0 mm), and moderate grinding depth (0.5 mm) with a composite desirability of 0.817.

*Corresponding author's e-mail address: boadumian@gmail.com (Boadu, M.K.)

1.0 Introduction

The resilience and corrosion rate of aluminum alloy can be effectively predicted using various modelling approaches that account for multiple influencing factors. Ma *et al.* (2024) transformed the process parameters in Pulsating Hydraulic Fracturing (PHF) into sequence data, which serves as the input for a long short-term memory neural network (LSTM) model aimed at predicting the mechanical properties of aluminium alloy components post-PHF process. Additionally, prediction models utilising Random Forest (RF), Support Vector Regression (SVR), and Back Propagation Neural Network (BPNN) have been developed and compared to the LSTM model. Furthermore, a few-shot learning approach grounded in the constitutive model is introduced to forecast the properties of aluminium alloys.

In this study, three distinct machine learning-assisted approaches are employed to analyse the connection between alloy composition, process parameters, and mechanical properties of 7xxx aluminum alloy, with the aim of expediting the advancement of new materials ("Manipulation of Mechanical Properties of 7xxx Aluminum Alloy via a Hybrid Approach of Machine Learning and Key Experiments", 2022).

Ghanizadeh & Rahrovan (2016) used a feed-forward backpropagation neural network to estimate the resilient modulus of stabilised bases based on five input factors: the number of W-D cycles, the ratio of free lime to SAF (silica, alumina, and ferric oxide compounds in cementitious materials), the ratio of maximum dry density to optimum moisture content, confining stress, and deviator stress.

Guzman *et al.* (2024) explored the heat treatment conditions for 6061 aluminium alloy to improve its mechanical properties. The Taguchi design-of-experiments (DOE) methodology was applied to methodically assess the impact of solutionising temperature, solutionising time, ageing temperature, and ageing time on the alloy's tensile strength. Mechanical testing indicated a significant effect of both solutionising and ageing temperatures on the ultimate tensile strength of the alloy.

Mikhail *et al.* (1999) reported on the findings from a study that analysed and compared resilient modulus values obtained from lab tests with those determined by back-calculating falling weight deflectometer (FWD) data from the WesTrack initiative in northern Nevada.

Bataineh & Smadi (2022) explored how temperature and holding time affect the hardness and impact toughness of Al 6061 by employing the design of experiments (DOE) framework. The results from DOE-factorial experiments were examined using analysis of variance (ANOVA). A model based on artificial neural networks (ANN) was developed to forecast the hardness and impact toughness of the precipitation-hardened 6061 aluminum alloy. The findings showed that temperature, holding time, and their interaction were significant contributors to the hardness and impact toughness of Al 6061.

Pezo & Hudson (1994) conducted experimental research to create predictive models for the resilient modulus of nongranular materials. Two models were formulated; the first offers a rapid estimation of the resilient modulus using fundamental characteristics of the samples, while the second model consists of a set of curves that relate a normalised modulus to resilient axial strains and the plasticity index of the samples.

Li *et al.* (2024) introduced a model for predicting corrosion while taking into account the effect of an electric field. Using 6061 aluminum alloy as a case study, they determined the corrosion behaviour of the alloy both in the absence of an electric field and with an applied electric field of 20 kV/m. Their findings indicated that the corrosion rate of the aluminum alloy initially rises and then falls with increased corrosion time and that the corrosion rate with an electric field is higher than without it during the same period.

Srinivasan & Kollo (2023) forecasted the galvanic corrosion of aluminum alloy through accelerated laboratory electrochemical tests. The corrosion rate was derived from the galvanic current and the wetness duration. Additionally, surface morphology and elemental surface evaluations were performed to elucidate the corrosion process.

Corrosion rates for aluminum alloys were estimated using machine learning approaches, namely XGBoost, Random Forest, and artificial neural networks, achieving minimal error rates. The XGBoost method resulted in the most accurate prediction, achieving an R^2 value of 0.9968 (Özkavak & Tunay, 2024).

A corrosion damage prediction model for aluminum alloys was created, establishing a nonlinear relationship among maximum corrosion depth, fatigue performance, corrosion temperature, and corrosion duration based on MATLAB, utilising the BP (Back Propagation) algorithm of neural networks. This method allows for predicting the corrosion trends of aluminum alloys. Both four-layer and three-layer networks were employed, discussing the impact of the neural network structure on accuracy. The results illustrated that the four-layer network outperformed the three-layer network in precision (Tan, 2009).

Li *et al.* (2013) examined climatic factors and aluminum alloys' corrosion data across 10 atmospheric corrosion locations to develop a corrosion prediction model for aluminum alloys. The validity of this corrosion model was confirmed by employing a BP artificial neural network to learn, train, and simulate, and it was compared with the corrosion test outcomes of aluminum alloy samples from the 10 typical atmospheric corrosion testing sites. The findings indicate that a reliable forecasting model can be established using the BP artificial neural network, effectively predicting the corrosion rates of aluminum alloys at these 10 typical atmospheric corrosion testing locations.

He *et al.* (2019) introduced a technique for forecasting the corrosion levels of aluminum alloys by gathering electrochemical parameters during corrosion assessments, which facilitates a swift evaluation according to established standards, yielding high detection speed and minimal error.

Saber *et al.* (2021) conducted a study employing optimal regression techniques to forecast the corrosion rate (CR) of Al-Si alloys, discovering that the corrosion rate rises with increasing stirring speeds, peaking at a pH of 3.5, with Gaussian process regression yielding the most precise predictions.

Xiong *et al.* (2024) measured the corrosion potentials (Ecorr) and corrosion rates of 40 as-cast 7XXX Al alloys through potentiodynamic polarisation tests and immersion tests. They utilised chemical compositions and physical features to create a machine learning model to predict these parameters. Random Forest Regression (RFR) was employed for predicting Ecorr with features including Cu, Ti, Al, and Zn, while Gaussian Process Regression (GPR) was used for predicting the corrosion rate, utilising characteristics such as specific heat, latent heat of fusion, and the proportion of p-electrons.

Wang & Lv (2023) developed a prediction model for the corrosion rate of aluminum alloys using a general regression neural network optimised by the Multi-Verse Optimiser, incorporating input data regarding alloy composition and environmental factors to accurately forecast mass loss resulting from salt spray corrosion.

An experimental design provides a systematic approach for examining the impact of different factors on surface quality, resulting in a general model capable of precisely predicting surface conditions (Ouafi & Barka, 2011).

Factorial design allows for the assessment of the effect of multiple independent variables on an outcome using one experiment rather than performing multiple experiments with individual independent variables. Factorial studies also allow for the evaluation of interactions between study variables (Anderson *et al.,* 2023).

Generally, factorial designs use a two-way ANOVA to assess both the main and interaction effects, providing a clear statistical framework for interpreting the findings. This analysis facilitates an understanding of the individual and collective effects of independent variables on a dependent variable (Andrade, 2024).

By utilising the Desirability Function (DF) approach, a scale-free value ranging from 0 to 1 is assigned to each response to the issue through individual DFs, which are then combined to produce an overall DF with a value within the interval [0, 1], typically by averaging them arithmetically or geometrically to achieve a single objective for the multi-response problem (Ehrgott, 2005).

Numerous software packages, such as Minitab, JMP, Package Desirability, and Design-Expert, are used in industrial settings to implement DFs based on the type developed by Derringer and Suich for their multi-response optimisation support. The core idea of the Desirability Function (DF) approach is that if one of the responses in an industrial process, product, or system, characterised by multiple responses, falls outside the acceptable limits, the overall DF becomes undesirable.

The DFs defined by Derringer and Suich (1980) may exhibit non-differentiability at a target value within the acceptable bounds of the response, influenced by the values of the function's shape parameter.

Derringer (1994) introduced a weighted case for these Desirability Functions (DFs) as a method to enhance the assignment of relative significance (or priorities) to individual responses.

Ch'ng *et al.* (2005) proposed an approach based on the arithmetic mean aggregation of the defined linear individual DFs, which are continuous and differentiable throughout their range, maintaining desirability within the interval [0; 2].

The literature indicates that there are currently no models connecting the parameters of surface grinding—such as table speed, feed, and grinding depth—to the resilience and corrosion rate of AA7075 thin plate. The primary objective of this research is to address this gap by developing models that can predict and control the resilience and corrosion rate of AA7075 thin plates during surface grinding by utilising the general full factorial design method. The models will be optimised through the application of the Desirability Function (DF) approach.

2.0 Materials and Methods

2.1 Material

The material used for the research was a thin Aluminum 7075 thin plate. The dimensions for samples for the resilience test were 300 mm x 50 mm x 4 mm, and those for the corrosion rate were 50 mm x 20 mm x 4 mm. These dimensions were achieved after the sample preparation but were altered after the surface grinding operation with respect to the experimental design. The weight percent of Silicon, Iron, Zinc, Magnesium, Titanium, Copper, Chromium, Manganese, Lead and Aluminum are 0.40, 0.50, 5.10, 2.10, 0.20, 1.20, 0.18, 0.30, 0.05 and 89.97, respectively (B209, 2014). Aluminium 7075 has a tensile strength of 157.7 MPa and a yield strength of 146.1 MPa. It also has a total elongation of 9.4% and a uniform elongation of 4.2% and a Young's modulus of 14.08 GPa. The density is found to be 2.77 g/cm^3. The equivalent mass is 9.0 g.

2.2 Design of Experiment

The factorial design was utilised to conduct the experiment. The experiment was concerned with investigating the influence of different grinding parameters (such as table speed, feed and grinding depth) on resilience and corrosion rates. The experimental runs were replicated, and a total of 54 runs were obtained. The factorial design is shown in Table 1 with the low (0), medium (1) and high (2) levels utilised during the experiment.

Table 1
The 3^3 Experimental Design Levels (Boadu et al. 2026)

Variables	(0)	(1)	(2)
Vs (spm)	2.0	15.0	50.0
f (mm)	1.0	2.0	5.0
D (mm)	0.2	0.5	1.0

The geometrical representation of a 3^3 factorial design is shown in Figure 1. The numbers denote the experimental runs.

Figure 1
Geometrical Representation of 3^3 Factorial Design (Vaxevanidis et al., 2015)

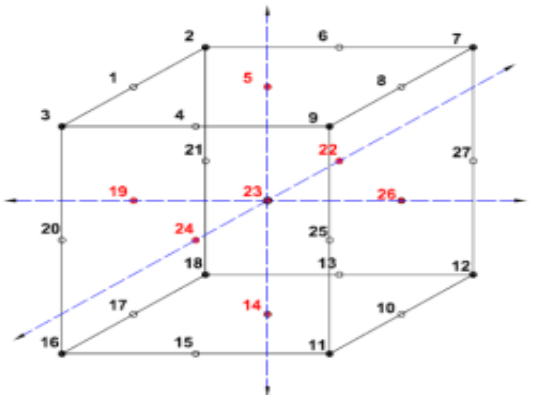

The design matrix for a 3^3 factorial design is shown as follows:

$$X = \begin{pmatrix}
0&0&0&0&0&0&0&0&0&0&0&0&0&0\\
0&0&1&0&0&1&2&1&2&1&2&1&2\\
0&0&2&0&0&2&1&2&1&2&1&2&1\\
0&1&0&1&2&0&0&1&1&1&1&2&2\\
0&1&1&1&2&1&2&2&0&2&0&0&1\\
0&1&2&1&2&2&1&0&2&0&2&1&0\\
0&2&0&2&1&0&0&2&2&2&2&1&1\\
0&2&1&2&1&1&2&0&1&0&1&2&0\\
0&2&2&2&1&2&1&1&0&1&0&0&2\\
1&0&0&1&1&1&1&0&0&1&1&1&1\\
1&0&1&1&1&2&0&1&2&2&0&2&0\\
1&0&2&1&1&0&2&2&1&0&2&0&2\\
1&1&0&2&0&1&1&1&1&2&2&0&0\\
1&1&1&2&0&2&0&2&0&0&1&1&2\\
1&1&2&2&0&0&2&0&2&1&0&2&1\\
1&2&0&0&2&1&1&2&2&0&0&2&2\\
1&2&1&0&2&2&0&0&1&1&2&0&1\\
1&2&2&0&2&0&2&1&0&2&1&1&0\\
2&0&0&2&2&2&2&0&0&2&2&2&2\\
2&0&1&2&2&0&1&1&2&0&1&0&1\\
2&0&2&2&2&1&0&2&1&1&0&1&0\\
2&1&0&0&1&2&2&1&1&0&0&1&1\\
2&1&1&0&1&0&1&2&0&1&2&2&0\\
2&1&2&0&1&1&0&0&2&2&1&0&2\\
2&2&0&1&0&2&2&2&2&1&1&0&0\\
2&2&1&1&0&0&1&0&1&2&0&1&2\\
2&2&2&1&0&1&0&1&0&0&2&2&1
\end{pmatrix} \quad (1)$$

2.3 Experimental Procedure

The Elliot 921 Hydraulic Surface Grinding Machine was employed to grind the Aluminum 7075 plates using the diamond grinding wheel with dimensions of 200 x 25 x 76.2 mm and a grit size of 80 m. The aluminum workpiece was held firmly by the clamp (which was also held in place by the magnetic chuck) to ensure it was stable and properly supported to prevent any movement or vibrations during grinding. Before the surface grinding process started, the operating conditions for the machine were set to ensure an efficient and safe surface grinding operation. The spindle speed was kept constant at 2140.0 rpm. The grinding parameters, such as table speed, feed, and grind depth, were varied based on the experimental design shown in Table 1. No coolant was used during the surface grinding process. The grinder was turned on, and the diamond grinding wheel was brought in contact with the aluminum workpiece. Grinding was done by applying light and even pressure. The surface grinding process was closely monitored to ensure even surface grinding of the plate and also to check for any signs of discolouration, excessive heat, or sparks. The process was repeated for the other samples of the plate.

Figure 2

Image for the Experimental Set-up

Figure 2 showcases an image of the experimental set-up of the surface grinding process. In this research, the tensile test was used to determine the mechanical properties of the samples. The 2000 kN Servo-Hydraulic Testing Machine, DI-CP/V2, was employed. The resilience, *Ur* was computed from mechanical properties results by the relation:

$$Ur = \frac{1}{2}\sigma_y\varepsilon_y = \frac{1}{2}\sigma_y\left(\frac{\sigma_y}{E}\right) = \frac{{\sigma_y}^2}{2E} \quad (2)$$

Where E is the modulus of elasticity; σ_y is the yield strength at 0.2% strain offset and $\varepsilon_y$is the yield strain.

The potentiodynamic polarisation test was also employed to determine the corrosion properties of the samples. The CorrTest Electrochemical Workstation was employed. The corrosion rate, *CR* was computed from the electrochemical results as:

$$CR = 3.27\,x\,10^{-3}\,\frac{i_{corr}EW}{\rho} \quad (3)$$

Where *EW* is the equivalent weight, I_{corr} is the corrosion current density and ρ is the density of the corroding material.

2.4 Analysis of Statistical Data

2.4.1 The 3^3 *Design Model*

The 3^3 design model consists of three factors, each at three levels. The model for such an experiment is given as follows:

$$Y_{ijk} = \mu + A_i + B_j + AB_{ij} + C_k + AC_{ik} + BC_{jk} + ABC_{ijk} + \varepsilon_{ijk} \quad (4)$$

Where:

Y_{ijk} represents the observed response (such as resilience and corrosion rate).

μ denotes the overall mean that is independent of the treatment effect or intercept (the average response across all observations).

A_i refers to the effect associated with the i^{th} level of factor A (table speed).

B_j indicates the effect related to the j^{th}level of factor B (feed).

AB_{ij} signifies the interaction effect between the i^{th} level of factor A and the j^{th} level of factor B.

C_k represents the effect of the k^{th} level of factor C (grinding depth).

AC_{ik} denotes the interaction effect between the i^{th} level of factor A and the k^{th} level of factor C.

BC_{jk} refers to the interaction effect between the j^{th} level of factor B and the k^{th} level of factor C.

ABC_{ijk} signifies the interaction effect involving the i^{th} level of factor A, the j^{th} level of factor B, and the k^{th} level of factor C.

$\varepsilon_{ijk}$is the random error associated with the observation yijk and is assumed to be independently and identically distributed as ~ (0, σ^2).

2.4.2 Estimation of Parameters

Analysis for specific factor effects demands the estimation of the parameters of ANOVA models such as blocks, treatments, interactions, error and total (Robert *et al.,* 2003).

The average response of each level of factor A is as follows:

$$\bar{A}_1 = \frac{1}{9}\sum_{j=1}^{3}\sum_{k=1}^{3} Y_{1jk} \quad (5)$$

$$\bar{A}_2 = \frac{1}{9}\sum_{j=1}^{3}\sum_{k=1}^{3} Y_{2jk} \quad (6)$$

$$\bar{A}_3 = \frac{1}{9}\sum_{j=1}^{3}\sum_{k=1}^{3} Y_{3jk} \quad (7)$$

The main effect of each level of factor A is as follows:

$$A_1 = \bar{A}_1 - \bar{Y} \quad (8)$$

$$A_2 = \bar{A}_2 - \bar{Y} \quad (9)$$

$$A_3 = \bar{A}_3 - \bar{Y} \quad (10)$$

Where:

$\bar{Y}$is the average of the responses for all treatments.

The average response of each level of factor B is as follows:

$$\bar{B}_1 = \frac{1}{9}\sum_{i=1}^{3}\sum_{k=1}^{3} Y_{1ik} \quad (11)$$

$$\bar{B}_2 = \frac{1}{9}\sum_{i=1}^{3}\sum_{k=1}^{3} Y_{2ik} \quad (12)$$

$$\bar{B}_3 = \frac{1}{9}\sum_{i=1}^{3}\sum_{k=1}^{3} Y_{3ik} \quad (13)$$

The main effect of each level of factor A is as follows:

$$B_1 = \bar{B}_1 - \bar{Y} \quad (14)$$

$$B_2 = \bar{B}_2 - \bar{Y} \quad (15)$$

$$B_3 = \bar{B}_3 - \bar{Y} \quad (16)$$

The average response of each level of factor C is as follows:

$$\bar{C}_1 = \frac{1}{9}\sum_{i=1}^{3}\sum_{j=1}^{3} Y_{1ij} \quad (17)$$

$$\bar{C}_2 = \frac{1}{9}\sum_{i=1}^{3}\sum_{j=1}^{3} Y_{2ij} \quad (18)$$

$$\bar{C}_3 = \frac{1}{9}\sum_{i=1}^{3}\sum_{j=1}^{3} Y_{3ij} \quad (19)$$

The main effect of each level of factor C is as follows:

$$C_1 = \bar{C}_1 - \bar{Y} \quad (20)$$

$$C_2 = \bar{C}_2 - \bar{Y} \quad (21)$$

$$C_3 = \bar{C}_3 - \bar{Y} \quad (22)$$

The average response of each combination of levels for factors A and B is as follows:

$$\overline{AB}_{ij} = \frac{1}{3}\sum_{k=1}^{3} Y_{ijk} \quad (23)$$

The interaction effect for A and B is as follows:

$$AB_{ij} = \overline{AB}_{ij} - \bar{A}_i - \bar{B}_j + \bar{Y} \quad (24)$$

The mean response of each set of levels for factors A and C is as follows:

$$\overline{AC}_{ik} = \frac{1}{3}\sum_{j=1}^{3} Y_{ijk} \quad (25)$$

The interaction effect for A and C is as follows:

$$AC_{ij} = \overline{AC}_{ik} - \bar{A}_i - \bar{C}_k + \bar{Y} \quad (26)$$

The mean response for each set of levels for factors B and C is as follows:

$$\overline{BC}_{jk} = \frac{1}{3}\sum_{i=1}^{3} Y_{ijk} \quad (27)$$

The interaction effect for B and C is as follows:

$$BC_{jk} = \overline{BC}_{jk} - \bar{B}_j - \bar{C}_k + \bar{Y} \quad (28)$$

The three-way interaction for A, B and C is as follows:

$$ABC_{jk} = Y_{ijk} - \overline{AB}_{ij} - \overline{AC}_{ik} - \overline{BC}_{jk} + \bar{A}_i + \bar{B}_j + \bar{C}_k - \bar{Y} \quad (29)$$

The coefficient of determination (R^2) is a statistical parameter that usually gives some relevant insights about the goodness of fit of a regression model. An R^2 of 1 means that the regression or design model completely fits the data. The formula for R^2 is given below:

$$R^2 = \frac{SS_{res}}{SS_{tot}} \quad (30)$$

where SS_{res} is the residual sum of squares and SS_{tot} is the total sum of squares:

$$SS_{res} = \sum_{i=1}^{n}(y_i - \hat{y})^2 \quad (31)$$

$$SS_{tot} = \sum_{i=1}^{n}(y_i - \bar{y})^2 \quad (32)$$

$$\bar{y} = \frac{1}{n}\sum_{i=1}^{n} y_i \quad (33)$$

n = number of observations
The adjusted R^2 is defined as:

$$\bar{R}^2 = 1 - \frac{\frac{SS_{\text{res}}}{df_{\text{e}}}}{\frac{SS_{\text{tot}}}{df_{\text{i}}}} \quad (34)$$

where *df*i - degrees of freedom for the model (*df*i = *k*, where *k* is the number of predictors), *df*e - degrees of freedom for error (*df*e = *n* − *k* −1, *n* is number of observations, *k* is number of explanatory variables).
The predicted R^2 is expressed as:

$$R^2_{pre} = \frac{PRESS}{SST} \quad (35)$$

where *PRESS* is the prediction error sum of squares and *SST* is the total sum of squares:

$$PRESS = \Sigma (y_i - \hat{y}_{i(-i)})^2 \quad (36)$$

$$SST = (y_i - \bar{y})^2 \quad (37)$$

2.5 Optimisation Analysis Approach

2.5.1 Desirability Functions (DFs) of Derringer and Suich Type

The Minitab statistical tool utilises the desirability function approach in performing a multi-response optimisation as stated earlier. In our case, a multi-response optimisation for resilience and corrosion rate is performed simultaneously. In a multi-response optimisation scenario, the dependent variable Y(*x*) is defined as Y: $R^n \rightarrow$ R, where $x = (x_1, x_2, \ldots . x_n)^T$ is a vector of predictor parameters and $x_i \in$ R (for *i* = 1, 2,....n). A specific decision function (DF) d(Y(x)) normalises the dependent variable into the range [0; 1], meaning d: R → [0; 1].

Figure 3
One-Sided 2 And Two-Sided 2 Individual DFs of Derringer and Suich's Type (Öztürk et al., 2015)

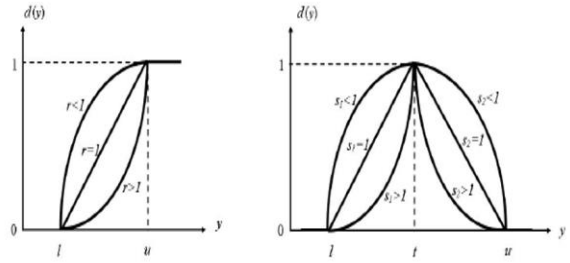

$d^Y(x) := d(Y(x)) = d(y)$ (38)

Where:
$R^n \rightarrow$ Y(*x*) with *y* belonging to R and $d^Y : R^n \rightarrow$ [0; 1].

This implies that the function d takes the value 0 for any unacceptable responses and reaches 1 for optimal expected responses. Decision functions are composite constructs of response functions, fundamentally based on the predictor parameters. two types: one-sided and two-sided, as stated by Derringer and Suich in 1980.

$$d(y) := \begin{cases} 0, & if\ y \le l, \\ \left(\frac{y-l}{u-l}\right) r, & if\ l < y \le l, \\ 1, & if\ y > u, \end{cases} \quad (38)$$

$$d(y) := \begin{cases} 0, & if\ y \le l \\ \left(\frac{y-l}{t-l}\right) s_1, & if\ l < y \le t \\ \left(\frac{y-u}{t-u}\right) s_2, & if\ t < y \le u \\ 0, & if\ y > u \end{cases} \quad (39)$$

In this context, *l* represents the minimum value and *u* represents the maximum desired value of *y*, while *t* denotes the highest acceptable value of *y*. The value of *r* used in Equation (38) is typically selected by the user. As *r* increases, y values that are nearer to *u* become more acceptable, and the opposite is true when *r* decreases. The terms s_1 and s_2 in Equation (39) have a similar significance in relation to *r*. There are three types of response optimisation: smaller-the-better, larger-the-better, and nominal-the-best. The interpretation of individual DFs for the larger-the-better scenario (one-sided DF) is represented in Equation (38). A similar interpretation can be offered for the smaller-the-better situation (one-sided DF). Equation (39) corresponds to the DFs in the nominal-the-best (two-sided DF) scenario. We consider a total of m responses in a multi-response optimisation scenario. After assessing the desirabilities of all responses using the corresponding functions outlined in (38) and (39), the overall DF, *D(y)*:$R^m \rightarrow$ [0; 1], is calculated using the geometric mean (Derringer and Suich, 1980):

$$D(y) := (d_1(y_1).d_2(y_2) \cdot \ldots \cdot d_m(y_m))^{\frac{1}{m}} \quad (40)$$

where $y := Y(x)$ and $Y(\cdot) := (Y1, Y2, \ldots . Ym)^T$.

In this context, it is evident that D(y) will fall within the range of [0; 1]. We denote the overall desirability as a function of *x* by $D^Y: R^n \rightarrow$ [0; 1] and define it by $D^Y(x) := D^Y(x))$, meaning that $D^Y(x)$ is equal to $d_1^Y(x) \cdot d_2^Y(x) \cdot \ldots \cdot d_m^Y(x)^{\frac{1}{m}}$. The function described in (38) represents a nonlinear composite objective function that

includes signomial terms. The use of the geometric mean to aggregate individual desirabilities results in the fundamental properties of DFs as a method. If we assume that the desirability, *d*, of a dependent variable, *y*, equals 0 at a specific factor *x*, the total desirability will also be 0 at that point, regardless of the values of other individual desirabilities at the same location. In the formulation of DFs, the interrelationships between the dependent variables are not considered, leading to the assumption that the responses operate independently of one another.

Figure4
*Asymmetric Nominal-the-Best Individual DF (*Akteke-Öztürk *et al., 2014)*

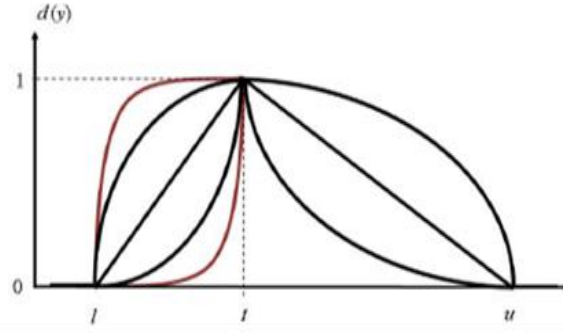

When the importance of each individual DF varies in determining the overall DFs, a weighting method is employed (Derringer, 1994):

$$D(y) : =\left(\prod_{j=1}^{m} d_j\,(y_j)^{w_j}\right)^{\frac{1}{\sum_{j=1}^{m} wj}} \quad (41)$$

The weighted overall desirability shares similar characteristics with the non-weighted version. Furthermore, if any of the dependent variables are deemed unacceptable at a certain factor vector, the overall desirability becomes zero at that juncture, meaning D (Y = 0), regardless of the desirabilities of other outcomes at that point. The decision-maker has the ability to set the weights based on the shapes of the desirability function curves. Typically, when determining the weights, it is wise to consider the relevance of both product and process responses in relation to one another. Figures 3 and 4 represent One-sided 2 and two-sided 2 Individual DFs of Derringer and Suich's type and Asymmetric nominal-the-best individual DF, respectively.

3.0 Results and Discussion

3.1 Influence of Surface Grinding Parameters on Resilience and Corrosion Rate

The results for the influence of surface grinding parameters on resilience and corrosion rate of the Aluminum 7075 plates is shown in Table 2. The main effects plot for resilience and corrosion rate are shown in Figures 5 and 6. The main effects plots denote the extent of the effects at low, intermediate and high levels.

Table 2
Influence of Surface Grinding Parameters on Resilience and Corrosion Rate

Runs	Vs	f	d	Ur		cR	
	spm	mm	mm	Pa		mm/a	
1	2.0	1.0	0.2	508000	826000	0.09	0.08
2	15.0	1.0	0.2	641000	642000	0.12	0.12
3	50.0	1.0	0.2	440000	409000	0.13	0.13
4	2.0	2.0	0.2	623000	629000	0.13	0.14
5	15.0	2.0	0.2	572000	556000	0.14	0.14
6	50.0	2.0	0.2	476000	472000	0.15	0.15
7	2.0	5.0	0.2	605000	607000	0.14	0.16
8	15.0	5.0	0.2	452000	450000	0.16	0.16
9	50.0	5.0	0.2	397000	396000	0.16	0.16
10	2.0	1.0	0.5	779000	871000	0.16	0.17
11	15.0	1.0	0.5	771000	744000	0.18	0.18
12	50.0	1.0	0.5	596000	599000	0.18	0.18
13	2.0	2.0	0.5	553000	645000	0.19	0.18
14	15.0	2.0	0.5	576000	574000	0.19	0.19
15	50.0	2.0	0.5	513000	534000	0.2	0.2
16	2.0	5.0	0.5	482000	465000	0.2	0.21
17	15.0	5.0	0.5	458000	447000	0.21	0.21
18	50.0	5.0	0.5	329000	404000	0.22	0.23
19	2.0	1.0	1.0	946000	706000	0.24	0.24
20	15.0	1.0	1.0	750000	725000	0.25	0.25
21	50.0	1.0	1.0	672000	628000	0.26	0.26

Runs	Vs	f	d	Ur		cR	
	spm	mm	mm	Pa		mm/a	
22	2.0	2.0	1.0	544000	541000	0.3	0.3
23	15.0	2.0	1.0	604000	648000	0.3	0.3
24	50.0	2.0	1.0	573000	576000	0.32	0.33
25	2.0	5.0	1.0	612000	627000	0.38	0.4
26	15.0	5.0	1.0	600000	506000	0.43	0.43
27	50.0	5.0	1.0	249000	392000	0.52	0.44

From Figure 5, the resilience is low (I47.6 Pa) when the table speed is 50 spm and moderate (595333 Pa) when the table speed is 15 spm. The resilience is also high (642722 Pa) when the table speed is 2 spm. This implies that the resilience increases by decreasing the table speed and vice versa. On the other hand, the resilience is low (471000 Pa) when the feed is 5 mm and moderate (567167 Pa) when the feed is 2 mm. The resilience is high (680722 Pa) when the feed is 1 mm. The data also shows that the resilience increases by decreasing the feed and vice versa. Lastly, the resilience is low (538944 Pa) when the grinding depth is 0.2 mm and moderate (574444 Pa) when the grinding depth is 0.5 mm. The resilience is high (605500 Pa) when the grinding depth is 1.0 mm. This implies that the resilience increases by increasing the grinding depth and vice versa.

According to Figure 6, the corrosion rate is low (0.21 mm/a) when the table speed is 2 spm and moderate (0.22 mm/a) when the table speed is 15 spm. The corrosion rate is also high (0.23 mm/a) when the table speed is 50 spm. This implies that the corrosion rate increases by increasing the table speed and vice versa. On the other hand, the corrosion rate is low (0.18 mm/a) when the feed is 1 mm and moderate (0.21 mm/a) when the feed is 2 mm. The corrosion rate is high (0.27 mm/a) when the feed is 5 mm. This data shows that the corrosion rate increases by increasing the feed and vice versa. Lastly, the corrosion rate is low (0.14 mm/a) when the grinding depth is 0.2 mm and moderate (0.19 mm/a) when the grinding depth is 0.5 mm. The corrosion rate is high (0.33 mm/a) when the grinding depth is 1.0 mm. This implies that there is a linear relationship between the grinding depth and the corrosion rate.

Figure 5

Main Effects Plot for Resilience

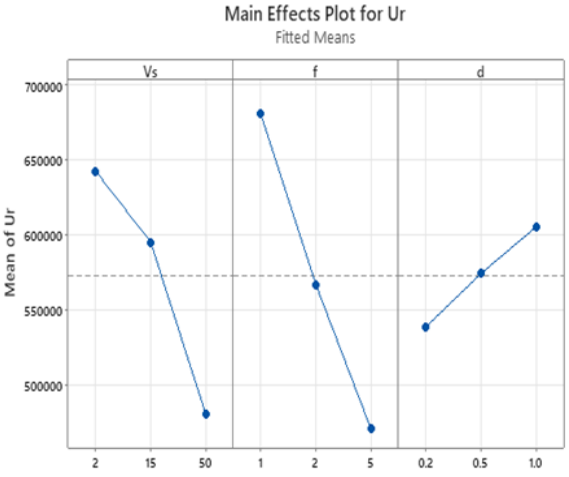

Figure 6

Main Effects Plot for Corrosion Rate

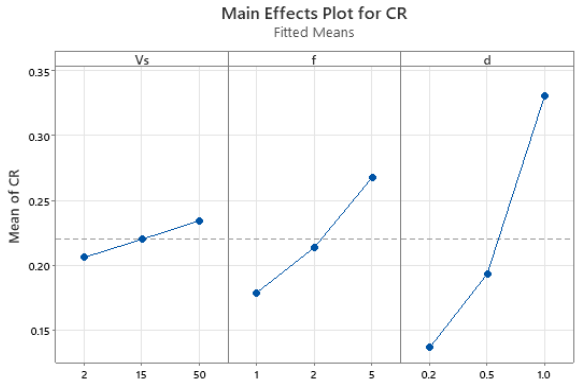

3.2 Identification of Important Factors

The interaction plot can be used to identify significant interactions. The interaction plots are shown in Figures 7 and 8. The plot examines the effects of combined factors or variables on resilience and corrosion rate. The plot examines two-way interactions because the three-way interactions are found to be insignificant. The blue represents the low, the moderate and the high levels of the surface grinding parameters, respectively. The lines, the dotted red lines and the dotted green lines represent the low, the moderate and the high levels of the surface grinding parameters, respectively.

From Figure 7, there is an interaction between the 2 spm table speed and the 2.0 mm feed. The rest of the levels for table speed and feed do not show any significant interaction. The levels for table speed and grinding depth do not interact. There is an interaction between the 2.0 mm feed and the 0.2 mm grinding depth. There is also an interaction between the 1.0mm feed and the 0.5 mm grinding depth. The rest of the levels of feed and grinding depth showed no significant interaction. Generally, the three-way interactions for the independent variables are found to be insignificant and thus are removed from the regression model. The two-way interactions of the predictors are found to be insignificant.

Figure 7
Interaction Plot for Resilience

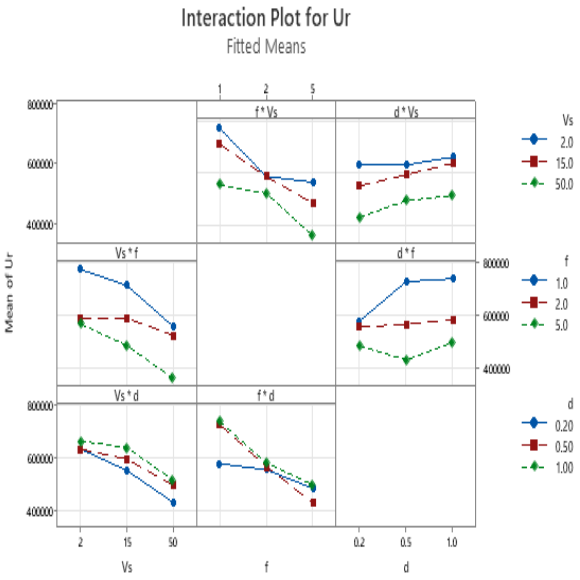

From Figure 8, there is no interaction between the levels of the grinding depth and the table speed. There is an interaction between the 2 spm table speed and the 2.0 mm feed. The rest of the levels of table speed and feed do not show any interaction. The 1.0 mm feed and the 1.0 mm grinding depth interact. The 1.0 mm feed and the 0.5 mm grinding depth interact. There is an interaction between the 2.0 mm feed and the 0.2 mm grinding depth. There is no interaction between the 2.0 mm feed and the 0.5 mm grinding depth. There is an interaction between the 2 spm table speed, the 1.0 mm feed and the 0.2 mm grinding depth. Generally, the two-way interactions and the three-way interactions for the predictors are found to be significant.

Figure 8
Interaction Plot for Corrosion Rate

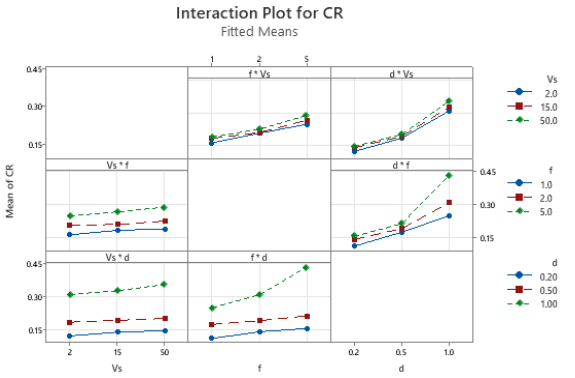

The Pareto charts for the standardized effects of table speed, feed and grinding depth at 95% confidence level are shown in Figures 9 and 10. The Pareto chart is utilised to identify the important factors that influence the responses (i.e., the resilience and the corrosion rate). The Pareto chart shows whether the main effects and the interaction effects of factors on resilience and corrosion rate are significant. An effect or factor becomes significant when it crosses the reference line. The effect or factor becomes insignificant if it does not cross the reference line.

From Figure 9, the feed has the highest significant absolute standardised effect of 8.68. The table speed also has a significant absolute standardised effect of 6.81. The interaction effect of feed and grinding depth has a significant absolute standardised effect of 2.78. The grinding depth has the lowest significant absolute standardised effect of 2.44. The table speed-feed interaction effects and table speed-grinding depth interaction effects are found to be insignificant, with absolute standardised effects of 1.88 and 0.34, respectively.

Figure 9
Pareto Chart of Standardized Effects on Resilience

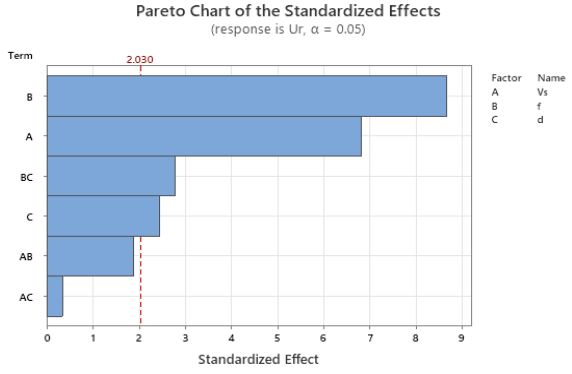

From Figure 10, the feed rate, the feed-grinding depth interaction, and the grinding depth all have the highest significant absolute standardised effect of 10.94. The feed rate during machining significantly influences surface roughness, which has a direct relationship with corrosion behaviour. Lower feed rates generally produce smoother surfaces, thereby minimising potential sites for corrosion initiation. For example, Gökkaya (2006) found that a feed rate of 0.10 mm/rev produced the least rough surface, which also meant that the corrosion rate was lower. Table speed has a significant, absolute, standardised effect of 6.37. The table speed-feed-grinding depth interaction has a significant absolute standardised effect of 2.34. The interaction effect of table speed and grinding depth has an insignificant absolute standardised effect of 2.01. The table speed-feed interaction effect is found to be insignificant, with an absolute standardised effect of 1.44.

Figure 10

Pareto Chart of Standardized Effects on Corrosion Rate

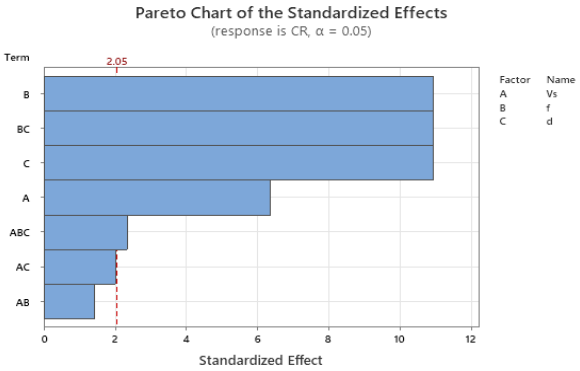

The coded coefficient table is also utilized to ascertain the significance of the interactions and factors on the response variables. Table 3 shows the coded coefficient table for resilience. Table 4 also shows the coded coefficients for corrosion rate. The factor or interaction effect is significant when the p-value is less than or equal to 0.05.

Table3

Coded Coefficients for Resilience

Term	Coef	SE Coef	T-Value	P-Value	VIF
Constant	572963	9167	62.50	0.000	
Vs					
2	69759	12964	5.38	0.000	1.33
15	22370	12964	1.73	0.093	1.33
f					
1	107759	12964	8.31	0.000	1.33
2	-5796	12964	-0.45	0.658	1.33
d					
0.2	-34019	12964	-2.62	0.013	1.33
0.5	1481	12964	0.11	0.910	1.33
Vs*f					
2 1	22185	18334	1.21	0.234	1.78
2 2	-47759	18334	-2.60	0.013	1.78
15 1	9074	18334	0.49	0.624	1.78
15 2	-1204	18334	-0.07	0.948	1.78
Vs*d					
2 0.2	24296	18334	1.33	0.194	1.78
2 0.5	-11704	18334	-0.64	0.527	1.78
15 0.2	-9148	18334	-0.50	0.621	1.78
15 0.5	-1815	18334	-0.10	0.922	1.78
f*d					
1 0.2	-69037	18334	-3.77	0.001	1.78
1 0.5	44463	18334	2.43	0.021	1.78
2 0.2	21519	18334	1.17	0.248	1.78
2 0.5	-2815	18334	-0.15	0.879	1.78

From Table 3, the constant is found to be notable with a p-value of 0.000. The 2.0 spm table speed is found to be important with a p-value of 0.000. The 15.0 spm table speed is found to be unimportant with a p-value of 0.093. The 1.0 mm feed is found to be important with a p-value of 0.000. The 2.0 mm feed is found to be important with a p-value of 0.658. The 0.2 mm grinding depth is found to be important with a p-value of 0.013. The 0.5 mm grinding depth is also found to be unimportant with a p-value of 0.910. The combined effect of the 2.0 spm table speed and

the 1.0 mm feed is found to be insignificant with a p-value of 0.234. The combined effect of the 2.0 spm table speed and the 2.0 mm feed is found to be notable with a p-value of 0.013. The combined effect of the 15.0 spm table speed and the 1.0 mm feed is found to be unimportant with a p-value of 0.624. The combined effect of the 15.0 spm table speed and the 2.0 mm feed is found to be insignificant with a p-value of 0.948. The combined effect of the 2.0 spm table speed and the 0.2 mm grinding depth is found to be insignificant with a p-value of 0.194. The combined effect of the 2.0 spm table speed and the 0.5 mm grinding depth is found to be insignificant with a p-value of 0.527. The combined effect of the 15.0 spm table speed and the 0.2 mm grinding depth is found to be insignificant with a p-value of 0.621. The combined effect of the 15.0 spm table speed and the 0.5 mm grinding depth is found to be insignificant with a p-value of 0.922. The interaction between the 1.0 mm feed and the 0.2 mm grinding depth is found to be notable with a p-value of 0.001. The combined effect of the 1.0 mm feed and the 0.5 mm grinding depth is found to be important with a p-value of 0.021. The combined effect of the 2.0 mm feed and the 0.2 mm grinding depth is found to be insignificant with a p-value of 0.248. The combined effect of the 2.0 mm feed and the 0.5 mm grinding depth is found to be insignificant with a p-value of 0.879.

Table 4
Coded Coefficients of Corrosion Rate

Term	Coef	SE Coef	T-Value	P-Value	VIF
Constant	0.22019	0.00165	133.77	0.000	
Vs					
2	-0.01407	0.00233	-6.05	0.000	1.33
15	-0.00019	0.00233	-0.08	0.937	1.33
f					
1	-0.04130	0.00233	-17.74	0.000	1.33
2	-0.00630	0.00233	-2.70	0.012	1.33
d					
0.2	-0.08352	0.00233	-35.88	0.000	1.33
0.5	-0.02685	0.00233	-11.54	0.000	1.33
Vs*f					
2 1	-0.00148	0.00329	-0.45	0.656	1.78
2 2	0.00685	0.00329	2.08	0.047	1.78
15 1	0.00463	0.00329	1.41	0.171	1.78
15 2	-0.00370	0.00329	-1.13	0.270	1.78
Vs*d					
2 0.2	0.00074	0.00329	0.23	0.824	1.78
2 0.5	0.00574	0.00329	1.74	0.093	1.78
15 0.2	0.00352	0.00329	1.07	0.295	1.78
15 0.5	0.00019	0.00329	0.06	0.956	1.78
f*d					
1 0.2	0.01630	0.00329	4.95	0.000	1.78
1 0.5	0.02296	0.00329	6.98	0.000	1.78
2 0.2	0.01130	0.00329	3.43	0.002	1.78
2 0.5	0.00463	0.00329	1.41	0.171	1.78
Vs*f*d					
2 1 0.2	-0.01185	0.00466	-2.55	0.017	2.37
2 1 0.5	-0.00019	0.00466	-0.04	0.969	2.37
2 2 0.2	-0.00019	0.00466	-0.04	0.969	2.37
2 2 0.5	-0.00519	0.00466	-1.11	0.275	2.37
15 10.2	0.00037	0.00466	0.08	0.937	2.37
15 1 0.5	0.00037	0.00466	0.08	0.937	2.37
15 2 0.2	-0.00130	0.00466	-0.28	0.783	2.37
15 2 0.5	0.00204	0.00466	0.44	0.665	2.37

In Table 4, the constant is found to be notable with a p-value of 0.000. The 2.0 spm table speed is found to be relevant, with a p-value of 0.000. The 15.0 spm table speed is found to be insignificant with a p-value of 0.937. The 1.0 mm feed is found to be relevant with a p-value of 0.000. The 2.0 mm feed is found to be relevant with a p-value of 0.012. The 0.2 mm grinding

depth is found to be important with a p-value of 0.000. The 0.5 mm grinding depth is also found to be relevant with a p-value of 0.000. The combined effect of the 2.0 spm table speed and the 1.0 mm feed is found to be insignificant with a p-value of 0.656. The combined effect of the 2.0 spm table speed and the 2.0 mm feed is found to be relevant, with a p-value of 0.047. The combined effect of the 15.0 spm table speed and the 1.0 mm feed is found to be insignificant with a p-value of 0.171. The combined effect of the 15.0 spm table speed and the 2.0 mm feed is insignificant, with a p-value of 0.270. The combined effect of the 2.0 spm table speed and the 0.2 mm grinding depth is found to be insignificant with a p-value of 0.824. The combined effect of the 2.0 spm table speed and the 0.5 mm grinding depth is found to be insignificant, with a p-value of 0.093. The combined effect of the 15.0 spm table speed and the 0.2 mm grinding depth is found to be insignificant with a p-value of 0.295. The combined effect of the 15.0 spm table speed and the 0.5 mm grinding depth is found to be insignificant with a p-value of 0.956. The combined effect of the 1.0 mm feed and the 0.2 mm grinding depth is found to be notable with a p-value of 0.000. The combined effect of the 1.0 mm feed and the 0.5 mm grinding depth is found to be notable with a p-value of 0.000. The combined effect of the 2.0 mm feed and the 0.2 mm grinding depth is found to be relevant with a p-value of 0.002. The combined effect of the 2.0 mm feed and the 0.5 mm grinding depth is found to be insignificant with a p-value of 0.171. The three-way interaction between the table speed at a low level (2.0 spm), the feed at a low level (1.0 mm) and the grinding depth at a low level (0.2 mm) is found to be significant with a p-value of 0.017. The remaining three-way interactions of the levels for the predictors are found to be insignificant.

The ANOVA table is also used to ascertain the significance of the models, interactions, and factors in the response variables. Tables 5 and 6 are the ANOVA tables for resilience and corrosion rate, respectively. The model, factor and interaction effects are significant when the p-value is less than or equal to 0.05 and insignificant when the p-value is more than 0.05.

Table 5
ANOVA for Resilience

Source	DF	Adj SS	Adj MS	F-Value	P-Value
Model	18	8.11849E+11	45102709877	9.94	0.000
Linear	6	6.86068E+11	1.14345E+11	25.20	0.000
Vs	2	2.49384E+11	1.24692E+11	27.48	0.000
f	2	3.96758E+11	1.98379E+11	43.72	0.000
d	2	39926037037	19963018519	4.40	0.020
2-Way Interactions	12	1.25781E+11	10481759259	2.31	0.027
Vs*f	4	43564962963	10891240741	2.40	0.069
Vs*d	4	9047407407	2261851852	0.50	0.737
f*d	4	73168740741	18292185185	4.03	0.009
Error	35	1.58823E+11	4537804233		
Lack-of-Fit	8	49736148148	6217018519	1.54	0.190
Pure Error	27	1.09087E+11	4040259259		
Total	53	9.70672E+11			

From Table 5, the regression model is found to be significant with a p-value of 0.000. There is a significant linear relationship between the grinding parameters and the resilience with a p-value of 0.000. The main effect of the table speed is significant with a p-value of 0.000. The main effect of the feed is significant with a p-value of 0.000. The main effect of the grinding depth is significant with a p-value of 0.020. The two-way interactions are found to be significant with a p-value of 0.027. The table speed-feed interaction is generally found to be insignificant with a p-value of 0.069. The table speed-grinding depth interaction is found to be insignificant with a p-value of 0.737. The feed-grinding depth interaction is generally found to be significant with a p-value of 0.009.

Table 6
ANOVA for Corrosion Rate

Source	DF	Adj SS	Adj MS	F-Value	P-Value
Model	26	0.486748	0.018721	127.97	0.000
Linear	6	0.437211	0.072869	498.09	0.000
Vs	2	0.007226	0.003613	24.70	0.000
f	2	0.072181	0.036091	246.70	0.000
d	2	0.357804	0.178902	1222.87	0.000
2-Way Interactions	12	0.046422	0.003869	26.44	0.000
Vs*f	4	0.001041	0.000260	1.78	0.162
Vs*d	4	0.001552	0.000388	2.65	0.055
f*d	4	0.043830	0.010957	74.90	0.000
3-Way Interactions	8	0.003115	0.000389	2.66	0.027
Vs*f*d	8	0.003115	0.000389	2.66	0.027
Error	27	0.003950	0.000146		
Total	53	0.490698			

According to Table 6, the regression model is significant with a p-value of 0.000. The correlation between the grinding parameters and the corrosion rate is very linear as shown by a p-value of 0.000. The main effect of table speed is also relevant with a p-value of 0.000. On the same note, the main effect of feed is significant with a p-value of 0.000. Additionally, the main effect of the grinding depth is observed to be significant, with a p-value of 0.000. The two-way interactions were found to be significant with a p-value of 0.000. Nevertheless, the table speed-feed interaction is insignificant with a p-value of 0.162. The interaction effect of the table speed and grinding depth is found to be insignificant with a p-value of 0.055. Conversely, an interaction of the feed and grinding depth has a significant effect with a p-value of 0.000. Finally, the three-way interaction between the predictors has also been found to be relevant, with a p-value of 0.027.

3.3 Generation and Evaluation of Regression Model

The 3^3 regression models for resilience, *Ur* and Corrosion Rate, *CR* are presented as;

$$U_r = 572963 + 69759Vs_2 + 22370Vs_{15} - 92130Vs_{50} + 107759f_1 - 5796f_2 - 101963f_5 - 34019d_{0.2} + 1481d_{0.5} + 32537d_{1.0} + 22185Vs_2f_1 - 47759Vs_2f_2 + 25574Vs_2 f_5 + 9074Vs_{15}f_1 - 1204Vs_{15}f_2 - 7870Vs_{15}f_5 - 31259Vs_{50} f_1 + 48963Vs_{50}f_2 - 17704Vs_{50}f_5 + 24296Vs_2d_{0.2} - 11704Vs_2d_{0.5} - 12593Vs_2d_{1.0} - 9148Vs_{15}d_{0.2} - 1815 Vs_{15}d_{0.5} + 10963Vs_{15}d_{1.0} - 15148Vs_{50}d_{0.2} + 13519Vs_{50} d_{0.5} + 1630Vs_{50} d_{1.0} - 69037f_1d_{0.2} + 44463f_1d_{0.5} + 24574f_1d_{1.0} + 21519f_2d_{0.2} - 2815f_2d_{0.5} - 18704f_2d_{1.0} + 47519f_5d_{0.2} -41648f_5d_{0.5} - 5870f_5d_{1.0}$$ (42)

$$CR=0.22019-0.01407Vs_2-0.00019Vs_{15}+0.01426 Vs_{50}-0.04130f_1-0.00630f_2+0.04759f_5-0.08352d_{0.2}-0.02685d_{0.5}+0.11037d_{1.0}-0.00148Vs_2f_1+0.00685Vs_2f_2-0.00537Vs_2f_5+0.00463Vs_{15}f_1-0.00370Vs_{15}f_2- 0.00093Vs_{15}f_5- 0.00315Vs_{50}f_1- 0.00315 Vs_{50}f_2 + 0.00630Vs_{50}f_5 + 0.00074Vs_2d_{0.2} + 0.00574Vs_2d_{0.5}-0.00648Vs_2d_{1.0}+0.00352Vs_{15}d_{0.2} +0.00019Vs_{15}d_{0.5}-0.00370Vs_{15}d_{1.0}-0.00426Vs_{50} d_{0.2}-0.00593Vs_{50}d_{0.5}+0.01019Vs_{50}d_{1.0}+0.01630f_1d_{0.2}+0.02296f_1d_{0.5}- 0.03926f_1d_{1.0} + 0.01130f_2d_{0.2} + 0.00463f_2d_{0.5}- 0.01593f_2d_{1.0}-0.02759f_5d_{0.2}-0.02759f_5d_{0.5}+0.05519f_5d_{1.0}-0.01185Vs_2f_1d_{0.2}-0.00019Vs_2f_1d_{0.5}+0.01204Vs_2f_1d_{1.0}- 0.00019Vs_2f_2d_{0.2}- 0.00519Vs_2f_2d_{0.5} +0.00537Vs_2f_2d_{1.0}+0.01204Vs_2f_5d_{0.2}+0.00537Vs_2f_5d_{0.5}-0.01741Vs_2f_5d_{1.0}+0.00037Vs_{15}f_1d_{0.2}+0.00037Vs_{15}f_1d_{0.5}- 0.00074Vs_{15}f_1d_{1.0}- 0.00130Vs_{15}f_2d_{0.2} +0.00204Vs_{15}f_2d_{0.5}-0.00074Vs_{15}f_2d_{1.0}+0.00093Vs_{15}f_5d_{0.2}-0.00241Vs_{15}f_5d_{0.5}+0.00148Vs_{15}f_5d_{1.0}+ 0.01148Vs_{50}f_1d_{0.2}-0.00019Vs_{50}f_1d_{0.5}-0.01130Vs_{50}f_1d_{1.0} + 0.00148Vs_{50}f_2d_{0.2} + 0.00315Vs_{50}f_2d_{0.5}- 0.00463Vs_{50}f_2d_{1.0}-0.01296Vs_{50}f_5d_{0.2}-0.00296Vs_{50}f_5d_{0.5} + 0.01593Vs_{50}f_5d_{1.0}$$ (43)

Where:

Ur = resilience; CR = corrosion rate; V_s = table speed in spm; f = feed in mm and d = grinding depth in mm

From Equation 42, the R-squared for the resilience regression model is 83.64% and shows that the model fits the data well. The R-squared (adj) is 75.22% and shows that the model explains 0.7522 of the variation of resilience. The

R-squared (pred) shows that the model as fitted can predict 61.05% of the variability in resilience. From Equation 43, the R-squared value for the corrosion rate regression model is 99.20% and shows that the model excellently fits the data. The adjusted R-squared value is 98.42%, and this means that the model explains 0.9842 of the variation in the corrosion rate. The predicted R-squared shows that the model can predict 96.78% of the variability in corrosion rate.

The residual plots illustrating resilience and corrosion rate can be seen in Figures 11 and 12, respectively. These residual plots consist of a histogram, plots versus order, versus fits, and a normal probability plot.

From Figure 11, the plots indicate that most of the data points align with the distribution line, thereby confirming the normality of the residuals. The standardised residuals plotted against fits help to determine if the variance remains constant, if there are any nonlinear relationships, or if outliers exist within the treatment data observations. The displayed plots reveal a random arrangement of standardised residuals around zero, indicating constant variance across all observations of each treatment data. The histograms of the standardised residuals reflect their distribution among all observations. The histograms do not exhibit a bell shape due to the number of intervals used for data grouping. Therefore, reference is made to the corresponding normal plot to verify its normal distribution characteristics, and from this viewpoint, it indicates that the standardised residuals are indeed normally distributed. The residuals versus order plots assess whether there are systematic influences in the data due to the period or sequence of data collection. The plot indicates that the residuals are randomly dispersed around zero. There is no evidence to suggest that the error terms are correlated, thus fulfilling the independence condition of effects. Overall, the residual plots for resilience are satisfactory, demonstrating that the models for resilience are satisfactory, demonstrating that the models developed are suitable and adequately represent the data.

Figure 11

Residual Plots for Resilience

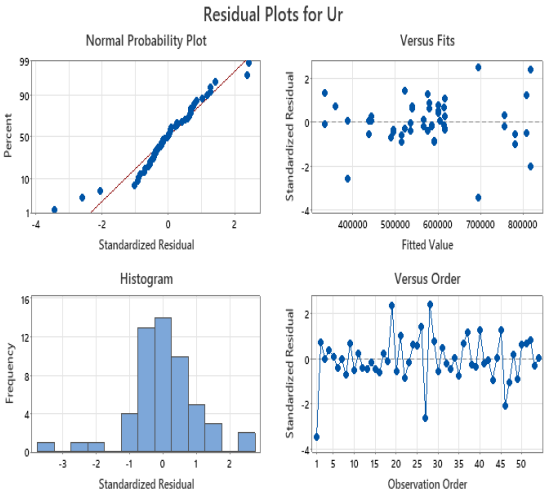

Based on Figure 12, the plots of the residuals of the corrosion rate provide useful data on the appropriateness of the regression model. The residual plots for the corrosion model show that the assumptions of the regression model are largely satisfied, which justifies the fitness of the regression model. However, the normal probability plot indicates that the standardised residuals follow the reference line with slight variations on both ends, indicating that the error distribution is more or less normal. This is supported by the histogram, which reveals that the residuals are concentrated around zero with a bell-shaped distribution that is almost symmetric with no extreme skewness and outliers. The plot of the residuals versus fitted values shows that the points are evenly spread around the values of zero, and thus, there is no apparent curvature or funnel-like shapes, and this ensures that the error variance is constant (homoscedasticity). This implies that there are no systematic features that are not explained by the model. The versus-order plot shows that there is an overall stability in the residuals as we progress through the order of observation, with a large spike at observation 30, and this could be attributed to some sort of disturbance in the experiment, but the order of observation of the residuals stabilises almost immediately, and it could be assumed that there is no sustained violation of independence. On the whole, the model can be justified by the analysis of the residuals, which show that even though there are slight anomalies, it can be easily used for

subsequent predictions of corrosion rate during surface grinding.

Figure 12
Residual Plots for Corrosion Rate

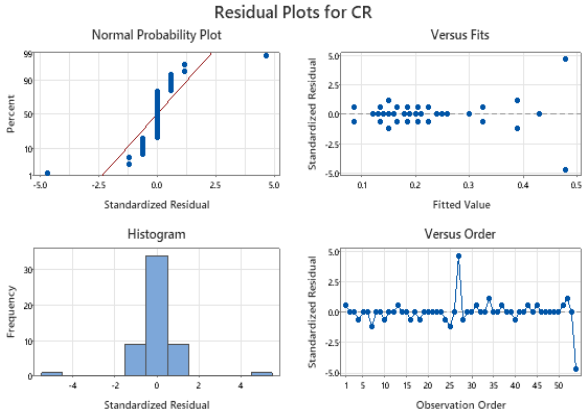

3.4 Multi-Response Optimisation for Resilience and Corrosion Rate

The multi-response optimisation plot is shown in Figure 13. The goal for the optimisation for resilience and corrosion rate is maximisation and minimisation, respectively. The desirability of resilience is found to be 0.826 with a fit of 825000 Pa and a standard error fit of 44946 Pa. The desirability of the corrosion rate is also found to be 0.807 with a fit of 0.17 mm/a and a standard error fit of 0.09 mm/a. The optimal settings for the predictors are found to be low table speed (2.0 spm), low feed (1.0 mm) and moderate grinding depth (0.5 mm). The composite desirability for resilience and the corrosion rate is 0.817, and this value implies that the optimal variable setting satisfies about 81.7% of the optimisation goals for resilience and corrosion rate.

Figure 13
Optimisation Plot for Resilience and Corrosion Rate

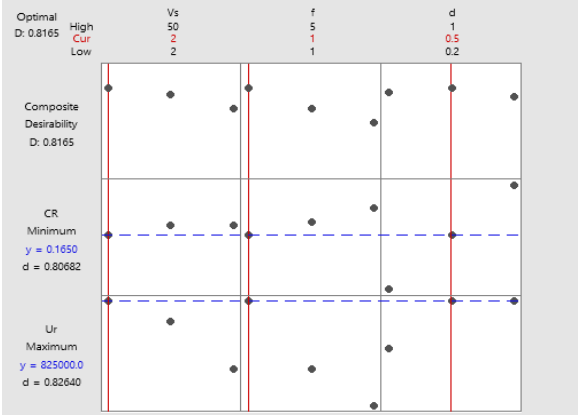

4.0 Conclusion

This research has proved that the parameters of surface grinding have a considerable impact on both the mechanical and corrosion characteristics of Aluminum 7075 thin plates. For resilience, the most significant factors were feed (absolute standardised effect = 8.68) and table speed (6.81); additionally, the interaction between feed and grinding depth was notable (2.78), whereas the interactions between table speed and feed, as well as table speed and grinding depth, were not significant. Regarding the corrosion rate, feed and its interaction with grinding depth had the strongest influence (10.94), followed by table speed (6.37) and the three-factor interaction (2.34), while the remaining interactions were not significant. Linear relationships were established between the grinding parameters and both resilience and corrosion rate. The regression model for resilience showed good performance (R^2 = 83.64%, adj. R^2 = 75.22%, pred. R^2 = 61.05%), whereas the regression model for the corrosion rate revealed excellent predictive precision (R^2 = 99.20%, adj. R^2 = 98.42%, pred. R^2 = 96.78%). The optimal settings were found to be low table speed (2.0 spm), low feed (1.0 mm), and moderate grinding depth (0.5 mm) with a composite desirability of 0.817, which indicates that the selected parameter combination satisfies 81.7% of the objectives for maximising resilience and minimising the corrosion rate.

5.0 Funding Declaration

This research received no specific grant from any funding agency in the public, commercial, or not-for-profit sectors.

6.0 Competing Interest

The authors state that none of their known financial conflicts or interpersonal connections might have had an impact on the work presented in this paper.

7.0 Conflict of Interest

We declare no conflict of interest.

8.0 Ethical Statement

This material is the authors' own original work,

which has not been previously published elsewhere.

9.0 References

Akteke-Öztürk, B., Weber, G. W., & Köksal, G. (2014). Desirability functions in Multi-response optimization. In *EURO Mini-conference on Optimization in the Natural Sciences* (pp. 129-146). Cham: Springer International Publishing.

Anderson, E. M., Niska, J. R., & Niska, E. E. (2023). Factorial design (pp. 327–330). *Elsevier BV*.

Andrade, C. (2024). Understanding Factorial Designs, Main Effects, and Interaction Effects: Simply Explained with a Worked Example. *Indian Journal of Psychological Medicine*,46(2), 175-177.

B209 (2014). Standard Specification for Aluminum and Aluminum-Alloy Sheet and Plate. *American Society for Testing and Materials, 100 Barr Harbor Dr., West Conshohocken, PA 19428*.

Bataineh, O., & Smadi, M. (2022). Using Artificial Neural Networks to Predict Hardness and Impact Toughness of Aluminum Alloy 6061- T6. *Materials Science Forum*, *1079*, 3–13.

Boadu, M.K., Agyei-Agyemang, A., Andoh, P.Y., Adam, F.W. (2026). Multi-Objective Optimization of Corrosion Current Density and Polarization Resistance of Surface-Ground AA7075 Thin Plate in 3.5 wt.% NaCl Solution. *Advances in Mechanical and Materials Engineering*, 43, 109-125.

Ch'ng, C.K., Quah S.H., and Low H.C. (2005). A New Approach for Multiple-Response Optimization. *Quality Engineering*, 17, 621-626.

Derringer, G. (1994). A balancing act, optimizing product properties. *Quality Progress*, 27, 51-57.

Derringer, G., and Suich, R. (1980). Simultaneous optimization of several response variables. *Journal of Quality Technology*, 12, 214-219.

Ehrgott, M. (2005). Multi-criteria Optimization. *Springer.*

Ghanizadeh, A. R., & Rahrovan, M. (2016). Application of Artificial Neural Network to Predict the Resilient Modulus of Stabilized Base Subjected to Wet-Dry Cycles. *Computations and Materials in Civil Engineering*, 1(1), 37–47.

Gökkaya, H. (2006). Experimental investigation of the effects of processing parameters on cutting force and surface roughness in machining of AA5052 Alloy. *Pamukkale University Journal of Engineering Sciences*, 12(3), 295–301.

Guzman, I. Ya., Granda-Gutiérrez, E. E., Cruz-González, C. E., Hernández-García, H. M., Díaz-Guillén, J. C., Flores-González, L., Praga-Alejo, R. J., & Martínez, D. I. (2024). Enhancing the Mechanical Properties of a 6061 Aluminum Alloy by Heat Treatment from the Perspective of Taguchi Design-of-Experiments. *Applied Sciences*, *14*(13), 5407.

He, M., Xie, L., Lu, Y., Jiangtao, W., Wang, X., Yan, C., & Liu, J. (2019). Rapid evaluation and prediction method for corrosion level of aluminum alloy.

Li, H., Lin, J., Liao, Y., & Bian, X. (2024). Aluminum alloy corrosion prediction model of power transmission line considering the influence of electric field. 1–4.

Li, L., Qiu, P., Xing, S. B., & Su, X. (2013). Research on Corrosion Rate Prediction of Aluminum Alloys in Typical Domestic Areas Based on BP Artificial Neural Network. *Advanced Materials Research*, 1088–1091.

Ma, H., Wang, P., Hu, Z., & Hua, L. (2024). Mechanical properties prediction of high-Strength aluminium alloy components formed under the PHF process. *MATEC Web of Conferences*, 401, 01008.

Manipulation of mechanical properties of 7xxx aluminum alloy via a hybrid approach of machine learning and key experiments. (2022). *Journal of Materials Research and Technology*, 19, 2483–2496.

Mikhail, M., Seeds, S. B., Alavi, S. H., & Ott, W. C. (1999). Evaluation of laboratory and back-calculated resilient moduli from the westrack experiment. *Transportation Research Record*, 1687(1687), 55–65.

Ouafi, A., & Barka, N. (2011). An integrated model for the prediction of surface condition in milling for aluminum alloys. *Revue De Metallurgie-Cahiers D*

Informations Techniques, 108(6), 357–368.

Özkavak, H., & Tunay, R. F. (2024). Predicting the Corrosion Rate of Al and Mg Alloys Coated by Plasma Spraying Method with Machine Learning. *Journal of Materials and Mechatronics,* 5(1), 130–142.

Pezo, R., & Hudson, W. R. (1994). Prediction Models of Resilient Modulus for Nongranular Materials. *Geotechnical Testing Journal*, 17(3), 349–355.

Robert, L. M., Richard, F. G., and James, L. H. (2003). Statistical and Analysis of Experiments. New York: *John Wiley and Sons Publication*.

Saber, D., Taha, I. B. M., & Abd El-Aziz, Kh. (2021). Prediction of the Corrosion Rate of Al–Si Alloys Using Optimal Regression Methods. *Intelligent Automation and Soft Computing*, 29(3), 756-769.

Srinivasan, R., & Kollo, T. (2023). Predicting Galvanic Corrosion of Aluminum Using Accelerated Laboratory Electrochemical Experiments. *Meeting Abstracts*. Tan, X. (2009). Prediction model for corrosion of aluminum alloys based on artificial neural network and analysis of the precision. *Journal of the Chinese Society of Corrosion and Protection*, 24(4), 218–221.

Vaxevanidis, N. M., Fountas, N. A., Koraidis, C., Koutsomichalis, A., & Psyllaki, P. (2015). Modeling of surface finish in turning of a brass alloy based upon statistical multi-parameter analysis. *Tribological Journal BULTRIB*, 5, 303-313.

Wang, Z., & Lv, S. (2023). A Salt Spray Corrosion Prediction Model for Aviation Aluminum Alloy Based on MVO-GRNN Algorithm. *Journal of Physics*, 2437(1), 012050.

Xiong, X., Zhang, N., Yang, J., Chen, T., & Niu, T. (2024). Machine Learning-Assisted Prediction of Corrosion Behavior of 7XXX Aluminum Alloys. *Metals*, 14(4), 401.